

Pairwise velocities in the Halo Model: Luminosity and Scale Dependence

Anže Slosar¹, Uroš Seljak^{2,3}, Argyro Tasitsiomi⁴

¹*Faculty of Mathematics and Physics, University of Ljubljana, Slovenia*

²*International Centre for Theoretical Physics, Trieste, Italy*

³*Department of Physics, Princeton University, Princeton, NJ 08544, USA*

⁴*Department of Astronomy & Astrophysics, Kavli Institute for Cosmological Physics, The University of Chicago, Chicago, IL 60637, USA*

Accepted —; received —; in original form 10 September 2021

ABSTRACT

We investigate the properties of the pairwise velocity dispersion as a function of galaxy luminosity in the context of a halo model. We derive the distribution of velocities of pairs at a given separation taking into account both one-halo and two-halo contributions. We show that pairwise velocity distribution in real space is a complicated mixture of host-satellite, satellite-satellite and two-halo pairs. The peak value is reached at around $1h^{-1}\text{Mpc}$ and does not reflect the velocity dispersion of a typical halo hosting these galaxies, but is instead dominated by the satellite-satellite pairs in high mass clusters. This is true even for cross-correlations between bins separated in luminosity. As a consequence the velocity dispersion at a given separation can decrease with luminosity, even if the underlying typical halo host mass is increasing, in agreement with recent observations. We compare our findings to numerical simulations and find a good agreement. Numerical simulations also suggest a luminosity dependent velocity bias, which depends on the subhalo mass. We develop models of the auto- and cross-correlation function of luminosity subsamples of galaxies in the observable $r_{\text{proj}} - \pi$ space and calculate the inferred velocity dispersion as a function of wave vector if dispersion model is fit to the redshift space power spectrum. We find that so derived pairwise velocity dispersion also exhibits a bump at $k \sim 1h/\text{Mpc}$.

Key words: cosmology: large scale structure of Universe

1 INTRODUCTION

Large redshift surveys such as SDSS (York et al. 2000) and 2dF (Percival et al. 2001) have provided us with a unique tool to probe the 3-dimensional structure of our Universe. The radial distances in those surveys are, however, modulated by the components of peculiar velocities along the line of sight. On large scales these velocities can be modelled using linear theory, as developed by Kaiser (1987). On small scales the velocities lead to radial stretching of groups and clusters, the so-called “fingers-of-God” (FOG). In principle this anisotropy in the observed structure can give us information on velocity structure of the Universe in addition to the spatial distribution of objects. Peculiar velocities of individual objects are sensitive to the amount and distribution of dark matter, but are difficult to measure in the absence of reliable distance estimators. The projected pairwise velocity differences, on the other hand, are much easier to measure from those surveys. Understanding the pairwise velocity distribution on all scales could therefore provide important dynamical information on the relation between the galaxies and surrounding dark matter.

The simplest approach to use dynamical information from pairwise velocities is to select isolated halo systems by some scheme (McKay et al. 2002; Prada et al. 2003; Brainerd & Specian 2003; van den Bosch et al. 2004). This process usually results in a selection of several system composed of a host galaxy and their satellites. Models can then be tested when many such isolated systems are compared “on average” to the theoretical predictions. The main advantage of this approach is that the selection scheme already labels the host and satellite galaxies, making the modelling somewhat easier. However, this approach also has several disadvantages: the number of suitable galaxies is very small (of the order of 1% of the total number of galaxies), the treatment of interlopers (galaxies that appear to be part of the system due to projection effects) can be difficult and model dependent, some of host galaxies may themselves be satellites of a larger system and, lastly, selecting isolated galaxy-satellite systems may not be representative of the dark matter-galaxy relation in general.

The alternative approach is to do as little preselection as possible and instead model the effects statistically within

a suitable model. This has the advantage of having large statistics and being more representative, given that by definition all galaxies are being used. This is the approach taken in this paper. We focus on the small scale correlations in redshift space and use the halo model (see e.g., Cooray & Sheth 2002) to provide an interpretation of the observations in the context of a physical model. Our approach thus focuses on statistical properties of the entire distribution of galaxies. Since the standard host-satellite separation is based on luminosity, this suggests that cross-correlation analysis between faint and bright galaxies might be especially effective in selecting central-satellite pairs and providing information about the halo structure. We thus follow Guzik & Seljak (2002) in working with narrow luminosity bins and perform both auto and cross-correlation analysis between them.

We assume the galaxies are either central galaxies in a halo or satellites, both of which need to have a specified conditional halo mass probability distribution. In this model the contributions to pairwise velocities come from host-satellite (host-sat from now on) and satellite-satellite (sat-sat from now on) pairs within the same halo and from two halo pairs (both host and satellite). A related approach with luminosity thresholds has been developed by Zheng et al. (2004), while van den Bosch et al. (2004) have focused on conditional luminosity function as a function of halo mass. We first build a model to describe the velocity structure of galaxies in the dark matter halos (Section 2). We perform this in terms of velocity distribution function, the probability that a pair of galaxies belonging to a given luminosity bin can be found at a given separation and has a given velocity component. This procedure is in spirit similar to that of Sheth (1996), although with a different emphasis and a more up to date version of the halo model. We show that less luminous galaxies can appear to move faster than their typical parent halo population even in the simplest halo model, in agreement with some observational results (Jing & Börner 2004).

In Section 3 we compare our model with numerical simulation. We calculate the correlation function in the $r_{\text{proj}} - \pi$ plane and use it to predict the dependence of σ_{12} parameter one would obtain by fitting it with a simple dispersion model (Section 4). The last section summarises our findings and concludes the paper. Throughout this paper, we assume a concordant flat cosmology with $\Omega_m = 0.3$, Hubble constant of $70 \text{ km s}^{-1} \text{ Mpc}^{-1}$ and $\sigma_8 = 0.9$.

2 PAIRWISE VELOCITIES IN HALO MODEL

We follow the standard halo model, which postulates that all galaxies live in the dark matter halos. The mass function $\eta = dn/dM$ of dark matter halos is most reliably estimated from numerical simulations and here we use the mass function fit from simulations (Jenkins et al. 2001)

$$\eta = \frac{dn}{dM} = 0.315 \frac{\rho_0}{M^2} \exp[-|\ln \sigma^{-1} + 0.61|^{3.8}] \frac{d \ln \sigma^{-1}}{d \log M}, \quad (1)$$

where σ is the variance in the linear density field at a given redshift, after smoothing with a spherical top-hat filter which encloses mass M in the mean. Each halo has a central galaxy and a Poisson distributed number of satellite galaxies. We consider galaxies with r-band luminosity between $L = -19$ and $L = -22$ and split them into three

luminosity bins of unit magnitude size. We always refer to a luminosity bin by its faint end magnitude. Additionally, we will refer to a sample of galaxies selected so that each pair contains one galaxy from luminosity bin L_i and one galaxy from the luminosity bin L_j as (L_i, L_j) . We will use symbols $n_C(M|L_i)$ and $n_{\text{NC}}(M|L_i)$ to denote the expectation value of the number of galaxies per halo which belong to the luminosity bin L_i and occupy central and non-central positions, respectively. Since every halo is assumed to have a central galaxy, the following must be true:

$$\sum_i n_C(M|L_i) = 1, \quad (2)$$

although some of these galaxies will fall outside the luminosity range we consider here.

We assume that the central galaxy is at the centre and at rest with respect to the parent halo. The satellite galaxies are distributed in the parent halo around the central galaxy. We assume this radial distribution follows the NFW profile (Navarro et al. 1996). We denote the probability of finding a galaxy at a distance between r and $r + dr$ in a halo of mass M as Φ_1 :

$$\Phi_1(r|M) \propto \frac{r}{r_s} \left(1 + \frac{r}{r_s}\right)^{-2}. \quad (3)$$

where $r_s = r_{\text{vir}}/c$, where c is concentration and $r_{\text{vir}}(M)$ is virial radius, which is defined as a radius of a sphere of mass M which has the average density 200 times critical density of the Universe. In simulations the subhalo distribution is less concentrated than the dark matter. Whether the same is true in the real universe is still a matter of an ongoing debate (Ghigna et al. 2000; Berlind & Weinberg 2001; Diemand et al. 2004; Collister & Lahav 2005; Yang et al. 2005; Nagai & Kravtsov 2005). In this work we assume the concentration parameter for the satellite galaxy distribution $c_g = 3$ and a cut-off at the $r_{\text{cut}} = 1.5r_{\text{vir}}$, which is in a reasonable agreement with simulations. Simulations show a weak dependence of the best-fit concentration on luminosity, but we neglect this effect here.

The probability of finding a galaxy belonging to the luminosity bin L_i in a halo with mass between M and $M + dM$ can be split into contribution from central and satellite galaxies:

$$P(M|L_i)dM = (1 - \alpha)P_C(M|L_i) + \alpha P_{\text{NC}}(M|L_i), \quad (4)$$

where α is the fraction of satellites among galaxies of luminosity L_i .

The probability distribution for the central galaxy is often assumed to be a δ function. Here we assume a slightly more realistic model and introduce a Gaussian spread around the mean value of $\log M$ (hereafter we assume log to be base 10). Although real distributions are asymmetric, especially at higher luminosities, it is a useful first-order correction. Therefore,

$$P_{C,i}(M) = G(\log M; \log M_{0,i}, \sigma_{v,i}), \quad (5)$$

where $G(x; \mu, \sigma)$ denotes a Gaussian distribution with mean μ and dispersion σ .

Following Mandelbaum et al. (2004) the distribution for $P_{\text{NC},i}$ is assumed to reflect a double power law for the

number of satellites per halo:

$$P_{\text{NC},i}(M) = \begin{cases} 0 & M < M_{0,i} \\ \propto \eta M^2 & M_{0,i} < M < 3M_{0,i} \\ \propto \eta M & \text{otherwise} \end{cases} \quad (6)$$

Constants of proportionality are chosen so that the function is continuous and normalised and give the overall satellite fraction $\alpha_i = 0.2$. Based on simulations we choose the following canonical values for $M_{0,i}$: $M(-19) = 5 \times 10^{11} h^{-1} M_\odot$, $M(-20) = 2 \times 10^{12} h^{-1} M_\odot$, $M(-21) = 1 \times 10^{13} h^{-1} M_\odot$ and fix $\sigma_{v,i} = 0.2$.

The total number of galaxies is given by the product of the number of halos and the number of galaxies per halo and therefore

$$P_{\text{C}}(M|L_i) = \frac{\eta n_{\text{C}}(M|L_i)}{\int \eta n_{\text{C}}(M|L_i) dM} = \frac{\eta n_{\text{C}}(M|L_i)}{N_{\text{C},i}}, \quad (7)$$

$$P_{\text{NC}}(M|L_i) = \frac{\eta n_{\text{NC}}(M|L_i)}{\int \eta n_{\text{NC}}(M|L_i) dM} = \frac{\eta n_{\text{C}}(M|L_i)}{N_{\text{NC},i}}, \quad (8)$$

$$(9)$$

where $N_{\text{C},i}$ and $N_{\text{NC},i}$ denote the total number density of galaxies belonging to a central/non-central class and belonging to the luminosity bin L_i . The fraction of non-central galaxies α_i is therefore given by:

$$\alpha_i = \frac{N_{\text{NC},i}}{N_{\text{NC},i} + N_{\text{C},i}} = \frac{N_{\text{NC},i}}{N_i}. \quad (10)$$

Next we turn to the distribution of velocities. Let us then define the pairwise velocity distribution $P(v, r|L_i, L_j)$ as the probability that of all pairs between galaxies from luminosity bin L_i and galaxies from the luminosity bin L_j , we find one at separation r , whose velocity difference vectors has magnitude v . We emphasise that in our definition, this is an object-weighted quantity rather than volume weighted quantity. The pairwise velocity dispersion as a function of radius is then given by:

$$\sigma_2^2(r|L_i, L_j) = \frac{\int_0^\infty P(v, r|L_i, L_j) v^2 dv}{\int_0^\infty P(v, r|L_i, L_j) dv}. \quad (11)$$

Similarly the correlation function is given by:

$$1 + \xi(r|L_i, L_j) = \frac{\int_0^\infty P(v, r|L_i, L_j) dv}{4\pi r^2 N_i N_j} \quad (12)$$

The pairwise velocity has two contributions. Single halo contribution comes from pairs residing in a single halo and dominates at small distances ($\lesssim 1 h^{-1}$ Mpc), while the two halo contribution dominates at larger distances.

Therefore we can write

$$P(v, r, |L_i, L_j) = P^{1h}(v, r|L_i, |L_j) + P^{2h}(v, r|L_i, L_j). \quad (13)$$

We now investigate each contribution in turn.

2.1 One-halo contribution

The single halo contribution to the pairwise velocity distribution has contributions from pairs formed one from the central and one from the satellite galaxies (host-sat pairs, denoted as hs) and those coming from two satellite galaxies (sat-sat pairs, denoted as ss):

$$P^{1h}(v, r|L_i, L_j) = P_{\text{hs}}(v, r|L_i, L_j) + P_{\text{ss}}(v, r|L_i, L_j). \quad (14)$$

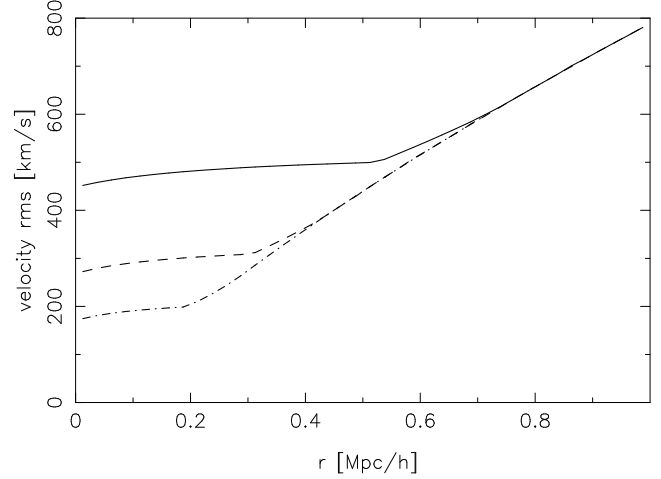


Figure 1. This figure shows the predictions for the one-point velocity dispersion relative to the centre of the halo for satellites selected from different luminosity bins for the halo model. Three luminosity bins are plotted: -21 (solid line), -20 (dashed line), -19 (dot dashed line).

The host-sat contribution is proportional to

$$P_{\text{hs}}(v, r|L_i, L_j) \propto \int [n_{\text{C}}(M|L_i) n_{\text{NC}}(M|L_j) + n_{\text{C}}(M|L_j) n_{\text{NC}}(M|L_i)] P_{1v}(v|r, M) \Phi_1(r|M) \eta dM. \quad (15)$$

Note that even though formally we have two terms inside square brackets of equation 15, if $L_i < L_j$ first term is negligible by equation 6.

The 1-particle velocity distribution $P_{1v}(v|r, M)$ is assumed to be Maxwellian. This is true for isothermal spheres and is in reasonable agreement with simulations. Therefore

$$P_{1v}(v|r, L_i) = M(v; b_v(L_i) \sigma_{\text{dm}}), \quad (16)$$

where $M(x; \sigma)$ denotes a Maxwell distribution corresponding to one-dimensional velocity variance σ_{dm} , which we take to be

$$\sigma_{\text{dm}} = 90 \text{ km s}^{-1} \left(\frac{M}{10^{12} h^{-1} M_\odot} \right)^{1/3}. \quad (17)$$

For the sake of simplicity we neglect the velocity bias at this stage, simply setting $b_v = 1$, but we return to this point below when we discuss the simulations. Note that we can simply switch between calculating the distribution of one-dimensional components of velocity and the distribution of speeds (lengths of the 3-dimensional velocity vectors) by replacing the Maxwell distribution with the corresponding one-dimensional Gaussian. We will use the superscript 1D to denote the distribution of one-dimensional components of velocity.

Similarly, one can write the sat-sat contribution as:

$$P_{\text{ss}}(v, r|L_i, L_j) \propto \int n_{\text{NC}}(M|L_i) n_{\text{NC}}(M|L_j) \times P_{2v}(v|M) \Phi_2(r|M) \eta dM. \quad (18)$$

In this equation Φ_2 denotes the probability that a pair of satellites is found at separation r . This corresponds to the self-convolution of the profile, which is most easily achieved

in the Fourier space:

$$\Phi_2(r|M) \propto r^2 \int \left[\int dr \Phi_1(r|M) \text{sinc}(kr) \right]^2 \text{sinc}(kr) k^2 dk. \quad (19)$$

It should be emphasised that the halo occupations are stochastic and a probability distribution is required to fully describe their statistical properties. We have implicitly performed the appropriate averages in the above expressions. In particular, the number of pairs for a Poisson distributed variable p is given by $\langle p(p-1) \rangle = \langle p \rangle^2$.

The function $P_{2v}(v|M)$ is used to denote the probability that the difference between velocity vectors has magnitude v . Because we assumed Maxwell distribution of velocities this is given simply by

$$P_{2v}(v|r, L_i) = M(v; \sqrt{2}\sigma_{\text{dm}}). \quad (20)$$

The above equations can be combined in the following expression for the pairwise velocity distribution:

$$\begin{aligned} P^{1h}(v, r|L_i, L_j) = & \int \left([(1 - \alpha_i)\alpha_j P_C(M|L_i) P_{\text{NC}}(M|L_j) P_{1v}(v|L_j) + \right. \\ & (1 - \alpha_j)\alpha_i P_C(M|L_j) P_{\text{NC}}(M|L_i) P_{1v}(v|L_i)] \Phi_1(r|M) + \\ & \left. \alpha_i \alpha_j P_{\text{NC}}(M|L_i) P_{\text{NC}}(M|L_j) \Phi_2(r|M) P_{2v}(v|L_i, L_j) \right) \\ & \times N_i N_j \frac{dM}{\eta}. \quad (21) \end{aligned}$$

This can be meaningfully compared to the one-point velocity distribution of galaxies at a distance r from the centre of its halo, that belong to the luminosity bin L_i . In our notation, this is given by:

$$P_1(v, r|L_i) = \int \alpha_i P_{\text{NC}}(M|L_i) \Phi_1(r|M) P_{1v}(v|L_i) N_i dM. \quad (22)$$

Note that the contribution due to the peculiar motion of the entire halo is not present in the above distribution.

Equations (21) and (22) show that true pairwise velocities tend to favour higher velocities compared to the one-point velocity distribution for two reasons. First, in a halo of a given mass, the velocity difference vectors of sat-sat pairs have a higher dispersion (by a factor of $\sqrt{2}$ if we neglect velocity bias). Second, the number of pairs contributed by a single halo scales as the square of the number of its satellites and since heavier halos contain more satellites, the pairwise velocity dispersion puts more weight towards heavier halos. This is encoded in the weighting factor for true pairwise velocity distribution, which is $\eta^{-1}dM$ compared to dM for the case of one-point velocity distribution.

2.2 Two-halo contribution

Two halo contribution comes from galaxies that are positioned in different halos. For host-host pairs, the correlation function follows the correlation function of parent halos, while for host-sat pairs the correlation function would have to be convolved with the halo profile and for the sat-sat it would have to be convolved with the halo profile twice. However, these effects are only important on small scales where one-halo term dominates. Hence, we ignore this effect and

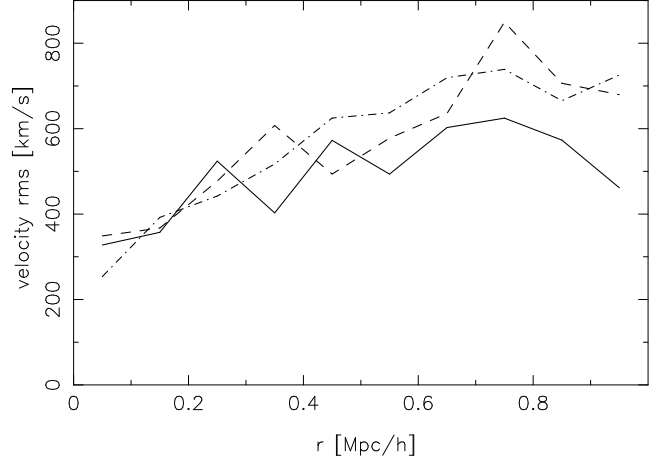


Figure 2. This figure shows the results for the one-point velocity dispersion relative to the centre of the halo in the simulation. Lines are labelled as in Figure 1.

assume that to a good approximation the three correlation functions are equivalent.

The correlation function for halos follows that of the linear theory, with the complication that the more massive halos are more correlated. This is modelled in a simple manner by introducing a bias factor for halos of mass M , given by Sheth & Tormen (1999)

$$b(\nu) = 1 + \frac{\nu - 1}{\delta_c} + \frac{2p}{\delta_c(1 + \nu^p)}, \quad (23)$$

where $\nu = [\delta_c/\sigma(M)]^2$ and $\nu' = a\nu$. The spherical overdensity at which a clump collapses δ_c is $\delta_c = 1.68$ for Einstein-de Sitter model and fitted values of other parameters are $a = 0.73$ and $p = 0.15$ (Mandelbaum et al. 2004). The cross-correlation between haloes of different masses is then given by:

$$\xi_{12}(r|M_1, M_2) = \xi_{\text{lin}}(r)b(M_1)b(M_2). \quad (24)$$

The probability of finding a pair of halos of masses between $M_{1,2}$ and $M_{1,2} + dM_{1,2}$, separated by a distance between r and $r + dr$ is therefore given by

$$(1 + \xi_{12}(r|M_1, M_2)) \eta(M_1)\eta(M_2)4\pi r^2. \quad (25)$$

Differences between host-host, host-sat and sat-sat pairs arise when considering their velocities. The velocity difference between host-host galaxy pairs arises purely due to velocity difference of their parent halos. The velocity distribution for halos is often assumed Maxwellian (Sheth & Diaferio 2001). In our simulations, it was observed that to a good approximation the velocity dispersion is given by $\sigma_{\text{halo}} = 455 \text{ km s}^{-1}$, independent of halo mass.

However, there are two factors that have to be taken into account when calculating the two-halo velocity dispersion term. First, neighbouring velocities are heavily correlated and consequently the probability distributions for velocities of two halos cannot be assumed independent. Second, if we select halos with a nearby neighbour and compare its velocity dispersion to population of halos without a nearby neighbour we find that the former is higher. This is simply due to the fact that halos that have close neighbours are more likely to live in a denser environment and thus have higher velocity dispersion. These effects are difficult

to model and we combine them into an effective dispersion suppression factor $s(r)$, so that the halo-halo probability for velocity difference can be written as:

$$p_{\text{hh}}^{2h}(v|r, M_1, M_2) = M(v; s(r)\sqrt{2}\sigma_{\text{halo}}) \quad (26)$$

We use the following fitting formula for $s(r)$:

$$s(r) = \begin{cases} \left(\frac{r}{r_0}\right)^\nu & r < r_0 \\ 1 & \text{otherwise,} \end{cases} \quad (27)$$

where $r_0 = 50h^{-1}$ Mpc and $\nu = 0.15$. The relative bias of haloes of different mass is ignored in this approximation.

When considering host-sat and sat-sat pairs we have to add the dispersion due to the satellite's peculiar motion with respect to its parent halo centre:

$$p_{\text{hs}}^{2h}(v|r, M_1, M_2) = M\left(v; [2\sigma_{\text{halo}}^2 s(r)^2 + \sigma_{\text{dm}}(M_2)]^{1/2}\right) \quad (28)$$

and

$$p_{\text{ss}}^{2h}(v|r, M_1, M_2) = M\left(v; [2\sigma_{\text{halo}}^2 s(r)^2 + \sigma_{\text{dm}}(M_1) + \sigma_{\text{dm}}(M_2)]^{1/2}\right). \quad (29)$$

Finally, we can assemble the 2-halo probability function:

$$\begin{aligned} P^{2h}(v, r|L_i, L_j) &= \int dM_1 \int dM_2 \\ &\times \left((1 - \alpha_i)(1 - \alpha_j) P_{\text{C}}(M_1|L_i) P_{\text{C}}(M_2|L_j) p_{\text{hh}}^{2h}(v|M_1, M_2) \right. \\ &\quad + P_{\text{NC}}(M_1|L_i) P_{\text{C}}(M_2|L_j) p_{\text{hs}}^{2h}(v|M_2, M_1, L_j, L_i) \\ &\quad + P_{\text{C}}(M_1|L_i) P_{\text{NC}}(M_2|L_j) p_{\text{hs}}^{2h}(v|M_1, M_2, L_i, L_j) \\ &\quad \left. + \alpha_i \alpha_j P_{\text{NC}}(M_1|L_i) P_{\text{NC}}(M_2|L_j) p_{\text{ss}}^{2h}(v|M_1, M_2) \right) \\ &\quad \times (1 + \xi_{12}(M_1, M_2)) N_i N_j 4\pi r^2 \quad (30) \end{aligned}$$

3 BASIC PREDICTIONS AND COMPARISON WITH SIMULATIONS

To check the validity of this model we compare it to a high-resolution numerical simulation. We use collision-less (dark matter only) simulation that is described in detail in Tasitsiomi et al. (2004), which has already been used for comparison with the halo model (Mandelbaum et al. 2004). We used the largest available simulation with the box size of $120h^{-1}$ Mpc and 512^3 particles and the cosmological model parameters were the same as described in the previous paragraph. The resolution of the simulation limits the analysis to halos heavier than $10^{11}h^{-1}M_\odot$ and thus we limit the discussion to galaxies that are brighter than -19 in the r-band magnitude.

The halos were identified using a variant of the Bound Density Maxima halo finder (Klypin et al. 1999); the details of this algorithm and the corresponding parameters can be found in Kravtsov et al. (2004). A catalog of dark matter halos is constructed so that every dark matter halo can have zero or more subhalos. Every halo is assumed to host a central galaxy. The maximum circular velocity is used as a proxy for halo mass for both halos and subhalos. Then the luminosities are assigned to each halo by matching the

cumulative velocity function $n(> V_{\text{max}})$ to the observed r-band cumulative luminosity function (Blanton et al. 2003). Since the mean SDSS redshift is ~ 0.1 the same redshift was used in simulation. More details can be found in Tasitsiomi et al. (2004).

3.1 One-point velocity dispersion

In Figure 1 we show the one-point velocity dispersion relative to the centre of the halo. This is calculated using the equation (11), but using the one-point velocity distribution given by the equation (21). In other words it is the root mean square velocity of satellites at distance r from the centre of their halo. Note that the so-defined one-point velocity dispersion is different from host-sat contribution to the pairwise velocity distribution: the latter additionally requires the luminosity of the central galaxy to belong to a chosen bin.

The velocity dispersion increases with increasing radius, even if we assume that the velocity dispersions is constant throughout a halo. This is simply a consequence of halo density weighting. The one-point velocity dispersion shows the expected behaviour of increasing velocity with the increasing luminosity at small separations. For separations from the centre of the halo that are larger than cut-off radius of halos of mass $M_{0,i}$ (for the luminosity bin L_i), the velocity dispersion increases faster with radius. At large enough separations all curves converge to the same one, following the distribution of velocities in halos weighted $M\eta$, where only halos with large enough cut-off radius can contribute.

Figure 2 shows the one-point velocity dispersion for galaxies in our simulation. We note that it does not show the expected behaviour. The more luminous galaxies live in heavier halos and thus they should be moving faster. This is a fairly robust prediction of the theory. The simulation shows that galaxies at the same distance from the centre move at an approximately constant speed at all radii, regardless of their luminosity. To understand this behaviour better we plot the one-point velocity dispersion relative to the centre of the halo in bins of the parent halo mass in Figure 3. We split the entire galaxy catalogue into four logarithmic bins according to the parent halo mass. We then split galaxies in each bin into three luminosity bins and plot the one-point velocity dispersion, where each individual point was plotted only if more than five galaxies contributed to it. We note the following: first, the approximation that the velocity dispersion is constant throughout the halo is roughly valid, in fact the velocity drops somewhat with distance as expected for an isotropic tracer in an NFW profile. This can also be a result of increased subhalo bias towards the centre (see e.g., Diemand et al. 2004). Second, the less luminous galaxies move faster than the more luminous galaxies even in halos of the same mass. This indicates a velocity bias that is increasing with decreasing luminosity. It is this bias that in Figure 2 conspires to nearly cancel the fact that one average more luminous galaxies come from more massive halos.

3.2 Pairwise dispersion

We first investigate how individual components contribute to the pairwise velocity dispersion. We plot these in Figure

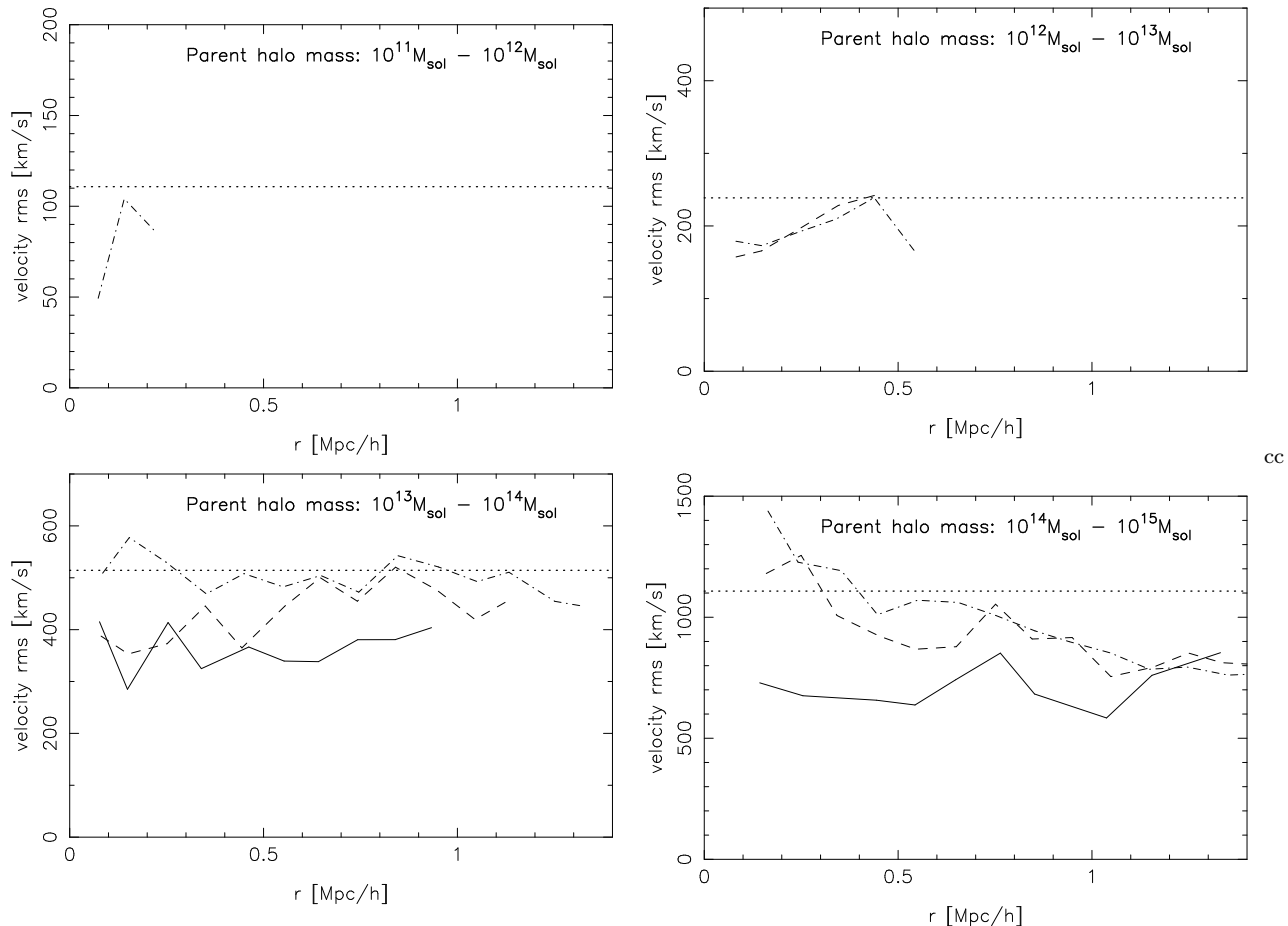


Figure 3. This figure shows the variation of the one-point velocity dispersion relative to the centre of the halo for galaxies belonging to a certain parent halo mass range. Line-styles are same as in the previous figures. The horizontal dotted line is the virial velocity dispersion of the mass corresponding the centre of the (log) mass bin. See text for discussion. Note that vertical axes have different ranges.

4. Thick lines are velocity dispersions of different components. The total velocity dispersion is the weighted combination of these individual dispersions. To ease visualisation we also plot individual components multiplied by the fraction of pairs of a given type.

At separations larger than $\sim 2h^{-1}$ Mpc, the two-halo contribution dominates. At smaller scales there is no regime where one type would dominate. The $(-21, -19)$ bin has a somewhat bigger contribution from the host-sat galaxy pairs, but not dominant enough to allow a clear separation by distance. The sat-sat contribution has considerably higher dispersion than the host-sat contribution. These pairs come from massive halos that have many light satellites and since dispersion is a pair weighted quantity, these dominate.

In Figure 5 we plot the combined contribution to the pairwise velocities as predicted by our model. At distances below $1h^{-1}$ Mpc we note that the galaxies selected from less luminous bins appear to move faster. This is explained by the fact that the fraction of host-sat pairs is decreasing as we go towards less luminous galaxies and sat-sat signal is almost independent of luminosity. This happens when the lower limit halo mass of satellites is low enough (i.e., the luminosity of galaxies involved is small enough) that the dominating sat-sat contribution, which probes $M^2\Phi_2(r|M)\eta$ (see Equation (21)), approaches a constant. In Figure 6 we plot

$M^2\eta$ showing that sat-sat pairs effectively pick up masses around $10^{14}h^{-1}M_\odot$ (though this of course depends on the power-law index in equation (6)). The $\Phi_2(r|M)$ factor additionally biases towards higher masses with increasing r .

When the two contributions are combined they result in a pronounced peak at around the typical size of the largest and therefore the most massive halos present. Such halos contain a lot of sat-sat pairs that move very fast and those dominate that region (at around $1h^{-1}$ Mpc). At larger distance we are dominated by many lighter halos with only a few members.

In Figure 7 we show the same total pairwise velocity dispersion as measured in our simulation. We note that the peak predicted by our simple model is also observed in the simulation.

To summarise the conclusions from this section, we have found that the pairwise velocity dispersion consists of 3 components, host-sat, sat-sat and 2-halo pairs and that there is no regime where one component would clearly dominate over the others.

The sat-sat component has the largest amplitude and drives the pairwise velocity dispersion peaks at around $1h^{-1}$ Mpc. The amplitude at the peak is fairly constant and determined by the second moment of the mass function, which is dominated by large clusters. Pairwise velocity

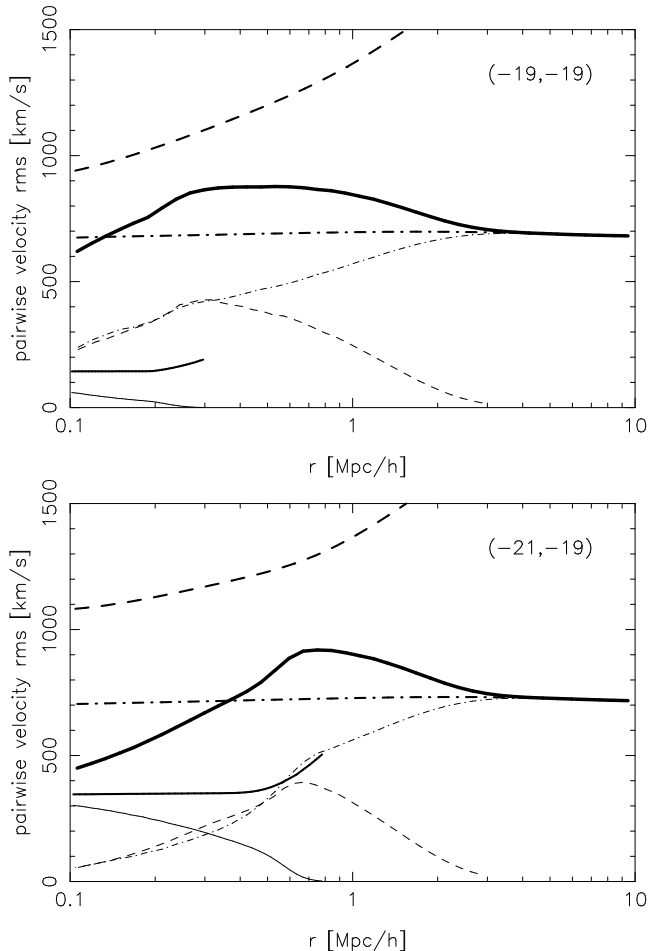


Figure 4. In this figure we show different contributions to the pairwise velocity dispersion. The very thick solid line is the total velocity dispersion, composed of host-sat pairs (thick solid), sat-sat pairs (thick dashed) and two-halo contribution (thick dot-dashed). These three contributions are weighted by the respective number of pairs. The thin lines show velocity dispersion multiplied by a fraction of a given component (so that thin lines add up to the thick line). We plot the $(-19, -19)$ (top) and $(-21, -19)$ (bottom) pairs. See text for discussion.

dispersion cannot be used to determine the typical halo mass of galaxies except on very small scales, where the number of pairs is small. This is true even for cross-correlation between different luminosity samples, which in principle is a better way to select host-sat pairs: while this does increase the host-sat to sat-sat ratio we find that it still does not sufficiently suppress the number of sat-sat pairs to make it a reliable tracer of host dark matter halo. Thus additional selections based on galaxy environment are needed if one wants to select a host-satellite sample only. Such additional selections may be difficult to model and reduce the size of the sample.

3.3 Adding velocity bias

We are now in position to rectify the main deficiency of our model with respect to the simulation, namely the velocity dependent bias. This was achieved by using the following values of the velocity bias as defined in Equation (16):

$b_v(-19) = 1.0$, $b_v(-20) = 0.9$, $b_v(-21) = 0.6$. These values were chosen so that the model reproduced the correct behaviour of the pairwise velocity dispersion. Results are plotted in Figure 8 (note that individual lines were shifted vertically by the same amount to make plot readable). The fit is remarkably good considering the simplicity of our model.

3.4 Fraction of satellites

A similar effect to the effect of velocity bias can be achieved by assuming a luminosity dependent fraction of satellites, i.e., $\alpha = \alpha(L)$. As Figure 9 shows, increasing the satellite fraction leads to an increase in velocity dispersion, as expected. It also makes the peak at $r = 1h^{-1}$ Mpc more pronounced, since that peak is caused by satellite-satellite pairs.

The numbers for the fraction of satellites in our simulation are 0.15, 0.20 and 0.23 for luminosity bins -19 , -20 and -21 respectively. Without introducing velocity bias it is possible to match the velocity dispersion of single-luminosity bins as shown in Figure 10. In this Figure we used the values as low as 0.06 for the most luminous galaxies, 0.17 for -20 galaxies and 0.20 for faintest galaxies considered.

However, as Figure 10 shows, the values of α that produce a decent fit for galaxy pairs of a single luminosity bin considerably decrease the goodness of fit for cross-bins. We also note that decreasing the fraction of satellites decreases the height of the peak at around $r \sim 1h^{-1}$ Mpc.

4 THE OBSERVABLE CORRELATION FUNCTION

4.1 Correlation function and the halo model

The pairwise velocity distribution we have been calculating so far is a basic distribution from which various other statistics can be calculated. It is not directly observable by itself. In the flat sky approximation, we see objects at various projected radii and their redshift encodes both their distance and their velocity component.

At large separations corresponding to two-halo contributions the galaxies experience infall that is well described by the linear theory beta model of Kaiser (1987). This results in squashing of the correlation function along the line of sight. The amount of distortion is parametrised by a single parameter $\beta = f/b$, where $f \sim \Omega_m^{0.6}$ is the linear growth factor and b is the linear bias. Ideally, one would like to incorporate the infall by considering a distribution of infall velocities. Note that Scoccimarro (2004) has shown that no distribution of infall velocities reproduces the beta model. Nevertheless, since beta model appears to be a good phenomenological model for description of infall, we include it here.

First we rewrite the probability of finding an object between r and $r + dr$ and having velocity v between v and $v + dv$ into cylindrical coordinates r_{proj} and z :

$$P_{\text{cyl}}(r_{\text{proj}}, z, v) = P\left(\sqrt{r_{\text{proj}}^2 + z^2}, v\right) \frac{r_{\text{proj}}}{2(r_{\text{proj}}^2 + z^2)} \quad (31)$$

The distribution in the $r_{\text{proj}} - \pi$ plane is then given by

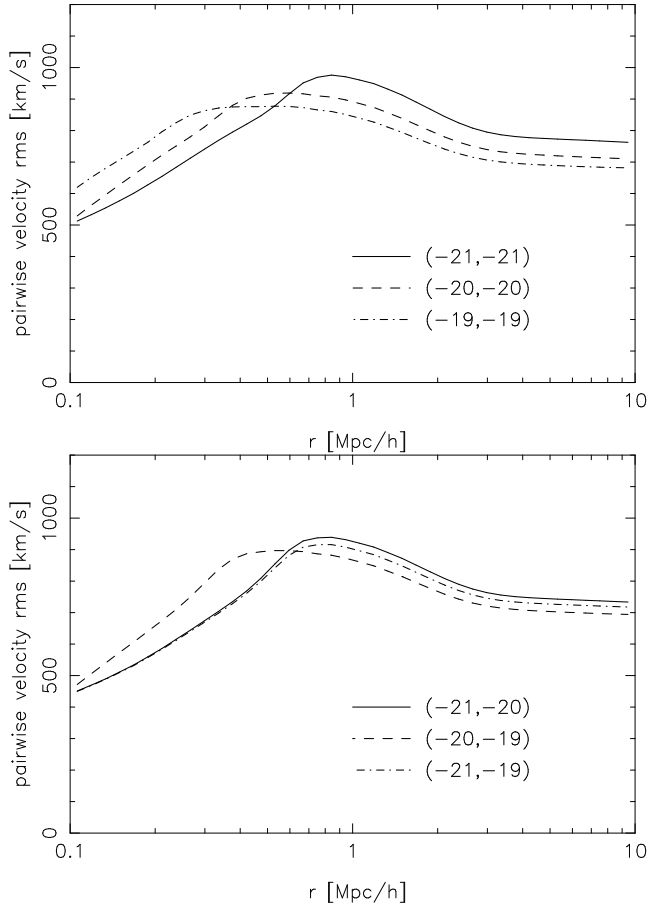


Figure 5. This figure shows the total prediction for the pairwise velocity dispersion for various luminosity bins shown in the legend. Distances below $1 h^{-1}$ Mpc are dominated by the one-halo term, while the two halo term dominates at larger distances.

$$P_{\text{obs}}(r_{\text{proj}}, \pi) = \int P_{\text{cyl}}^{\text{1D}}(r_{\text{proj}}, z, H_0(\pi - z)) \frac{dz}{H_0}. \quad (32)$$

We then calculate the observable correlation function by summing up contributions from 1-halo and 2-halo terms, following a procedure similar to many other works (White 2001; Seljak 2001; Kang et al. 2002; Cooray 2004):

$$\xi(r_{\text{proj}}, \pi) = \xi^{1h}(r_{\text{proj}}, \pi) + \xi^{2h}(r_{\text{proj}}, \pi) \quad (33)$$

The one-halo contribution is calculated from the Equation (32). This implicitly assumes that these systems are completely virialised and therefore not affected by the infall. The two-halo contribution, on the other hand, is calculated using standard dispersion model, which takes the following simple form in Fourier space:

$$P^S(\mathbf{k}) = P^R(k) \frac{(1 + \beta\mu^2)^2}{1 + k^2\mu^2\sigma_{12}^2/2}. \quad (34)$$

Here P^S and P^R denote the power spectrum in redshift space and real space respectively and μ is angle to the line of sight. The β parameter is calculated using bias predicted for a given luminosity bin from our model and velocity dispersion is given by the equation (11).

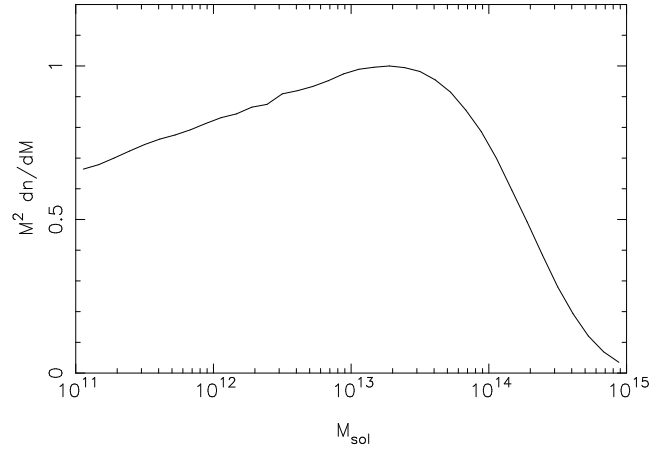


Figure 6. This figure shows ηM^2 as a function of M and shows which mass range is picked up by the sat-sat pairs in our model. See text for discussion.

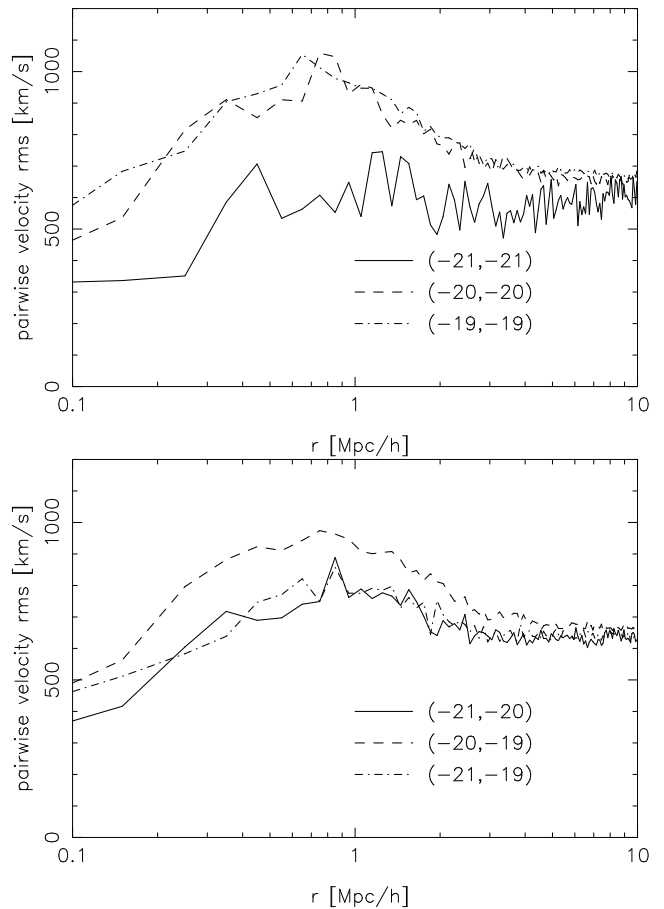


Figure 7. This figure shows the total pairwise velocity dispersion as measured in the numerical simulation.

4.2 Comparison to observations

Jing & Börner (2004) have found that less luminous galaxies in the 2dF redshift survey catalog appear to move faster. This conclusion is reached as follows. The correlation function of galaxies in the 2dF catalog is calculated for galaxies selected from various luminosity bins. This correlation function is used to calculate the redshift-space power spectrum

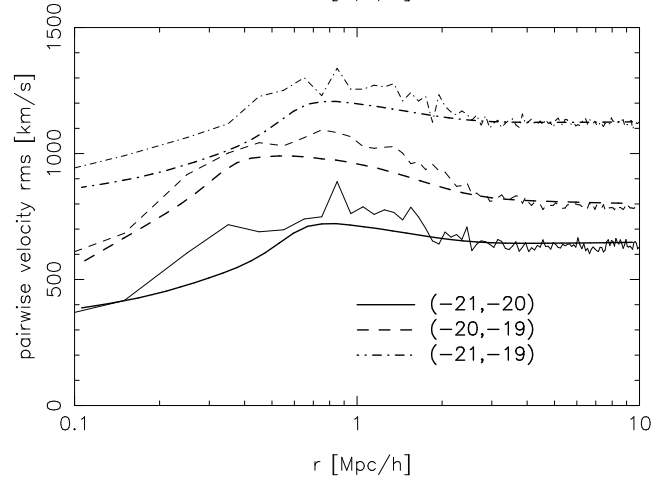
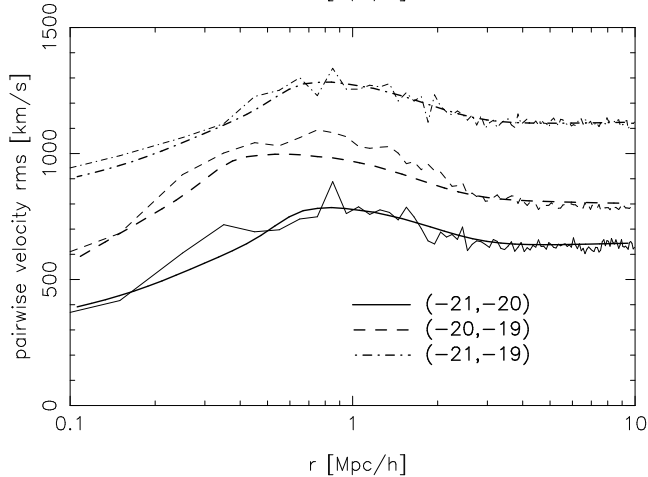
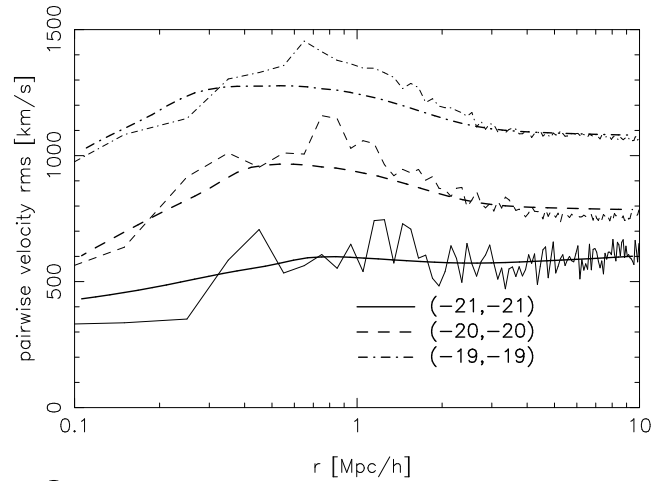
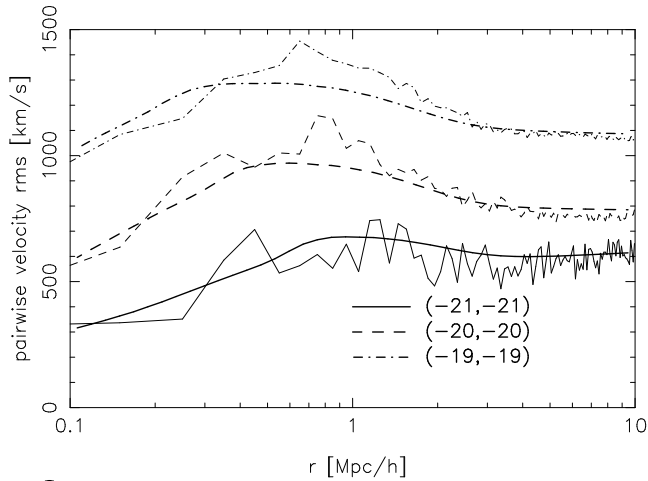


Figure 8. This figure shows the total pairwise velocity dispersion as measured in the numerical simulation compared to our model when velocity dependent bias has been added to the model. Jagged thin lines are simulation data and smooth thick lines the model prediction. Lines have been shifted vertically to ease visualisation.

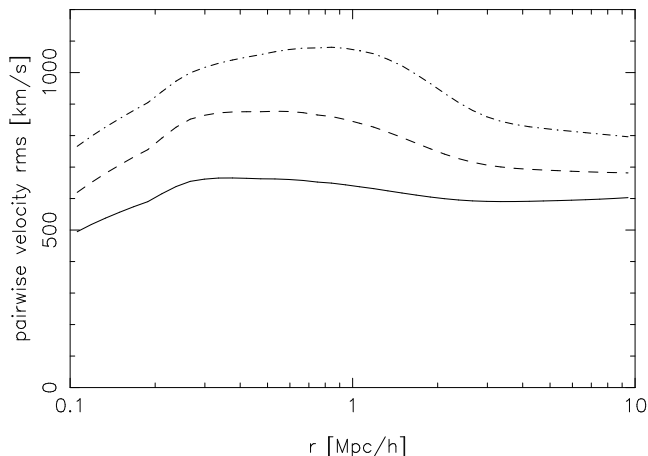


Figure 9. In this figure we plot the effect of changing the satellite fraction on the velocity dispersion. All lines correspond to $(-19,-19)$ pairs the satellite fraction α set to 0.4 (dot-dashed), 0.2 (dashed) and 0.1 (solid). Increasing the α parameter increases the overall velocity dispersion, but also makes the $1h^{-1}$ Mpc bump more pronounced.

Figure 10. Same as Figure 8, but with variable fraction of satellites used to match single-luminosity bins, instead of luminosity dependent velocity bias. See text for discussion.

$P^S(\mathbf{k})$. For each value of k the data is fit by fixing $\beta = 0.45$ and fitting for σ_{12} and $P(k)$.

There are three features in our model that can lead to an explanation of this effect. First, it is possible that the effect of pair weighting gives enough biasing towards more massive systems to explain the effect. As shown in Figure 11 the recovered velocity dispersion is non-monotonic, allowing for the possibility that velocity dispersion decreases with luminosity over some range, although the effect is not very pronounced and depends on the scale. Second, the addition of the luminosity dependent velocity bias works further in making less luminous galaxies appear to move faster. And third, allowing for satellite fraction to decrease with luminosity also leads to a decrease of velocity dispersion.

In order to meaningfully compare our predictions with Jing & Börner result we mimic their procedure. We predict a redshift space correlation function using our model, calculate the power spectrum and then fit the dispersion model to it. We also follow their procedure by fixing the β parameter to 0.45.

The main results of this exercise are plotted in Figures 11 and 12. We plot the recovered value of the σ_{12} parameter as a function of the wave vector k for three different luminosity bins. Figure 11 shows the behaviour for the simple model discussed throughout this paper. We note that the

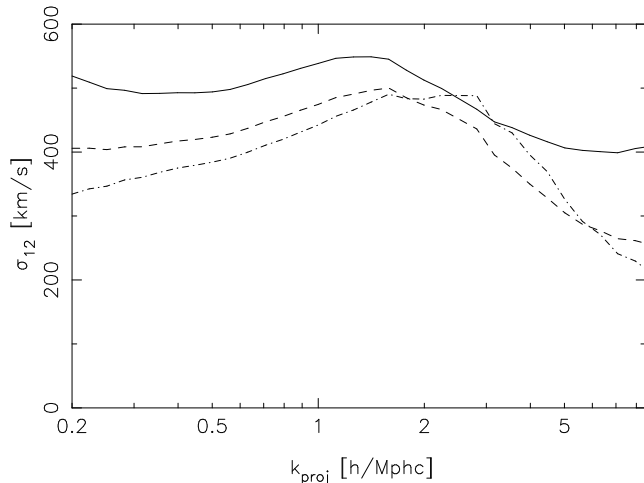


Figure 11. This figure shows the recovered σ_{12} parameter following the prescription used to analyse the data in (Jing & Börner 2004). Line styles as before.

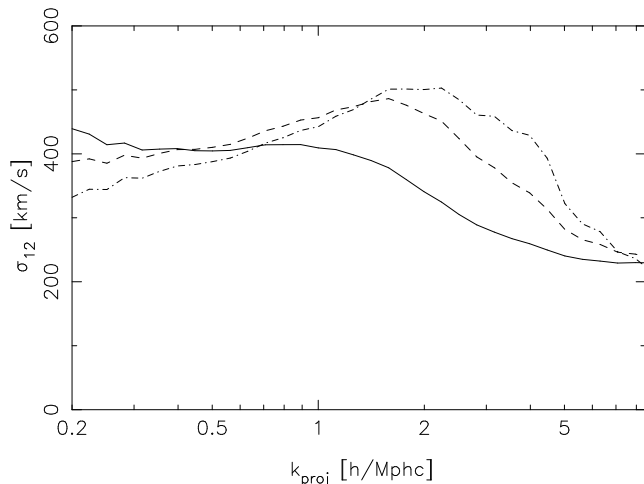


Figure 12. Same as figure 11, but a luminosity dependent velocity dispersion has been added to the model.

plot looks qualitatively the same as Figure 5 with an inverted horizontal axis. Here too, there is a typical bump at $k \sim 1h/\text{Mpc}$. The pair-weighting can result in less luminous galaxies appearing to move faster, but only at $k \gtrsim 2h/\text{Mpc}$ or so and therefore it is not clear whether this effect alone provides satisfactory explanation.

In Figure 12 we repeated the analysis, but added a luminosity dependent velocity bias that was used in section 3.3. Velocity biasing has the expected effect on the inferred velocity dispersions: galaxies of lower luminosity can indeed have a lower σ_{12} even at wave vectors as large as $1h/\text{Mpc}$.

We note that a similar analysis of the SDSS data (Li et al. 2005) shows qualitatively similar behaviour to our predictions plotted in Figure 12: a wide bump at around $1 - 2h/\text{Mpc}$ that becomes less pronounced for higher luminosities. The most luminous bins in that paper show an increase of σ_{12} with increasing k . We do not observe this behaviour here.

5 DISCUSSION AND CONCLUSIONS

In this paper we have investigated the pairwise velocity dispersion in the halo model and compared it to simulations. The distribution of velocities for galaxies separated by a certain distance in the real space is a pair weighted quantity and thus does not reflect the velocity structure of halos typically associated with galaxies of a given luminosity. In particular, for the pairs selected from either unequal luminosity bins or from equal luminosity bins (e.g., $(-20, -19)$, $(-19, -19)$, etc.) the main contribution comes from the sat-sat pairs. Since the halo mass distribution of satellites follows the halo mass function, which is exponentially suppressed on high mass end and has a power law at the low mass end, it probes a reasonably restricted range of parent halo mass around $10^{14} h^{-1} M_{\odot}$ and is nearly a constant. This, in combination with the fact that if one has a larger number of galaxies the number of sat-sat pairs relative to host-sat pairs increases, results in velocity dispersion which is not very luminosity dependent. The pairs selected so that one galaxy is more luminous than the other are also dominated by sat-sat pairs.

We have made predictions for redshift space correlation function of galaxies and fit it with the dispersion model, mimicking the observation procedure employed in Jing & Börner (2004) and in Li et al. (2005). In the latter work the measured σ_{12} in SDSS data has a qualitatively similar dependence on the wavenumber as predicted by our model. One of the main conclusions of these papers is that velocity dispersion declines with luminosity, which appears to contradict simple halo models. As mentioned even the simplest models do not suggest that there is a strong luminosity dependence, since most of the contribution comes from sat-sat pairs. Two other effects can give rise to velocity dispersion decreasing with luminosity. One is luminosity dependent velocity bias. In the simulation the effect that more luminous galaxies appear to move slower is clearly evident: in the halos of the same mass, the more luminous subhalos tend to move slower than their less luminous counterparts. Tidal stripping and tidal disruption have been suggested to explain the anti-bias of subhalo distribution (see e.g., Kravtsov & Klypin 1999; Diemand et al. 2004; Zentner et al. 2005) to the dark-matter distribution in a given halo and to explain the velocity bias of the subhalo population. Subhalos with lower orbital energy do not survive and one is left with halos that are on average faster. We note however that in these dark matter simulations one uses a simple prescription to link the luminosity of a galaxy with the circular velocity of the subhalo, which may be more complicated in the real world. Second effect that can give rise to velocity dispersion decreasing with luminosity is if satellite fraction also decreases with it. There is already some observational evidence for this from halo modelling of luminosity dependent galaxy correlation function Zehavi et al. (2005) and this explanation has also been put forth by Jing & Börner (2004). Both of these effects can therefore explain the observed trends and can be included in halo models. In summary, using auto and cross correlations between luminosity bins in redshift space to extract PVD is unlikely to provide us with simple information such as the mass and mass profile of the central galaxy halos, but is instead telling us more about the fraction of galaxies that are satellites and their velocity bias inside clusters.

ACKNOWLEDGEMENTS

We acknowledge useful discussions with Andrey Kravtsov. AS thanks Rachel Mandelbaum for helping with SDSS and simulation data. AS is supported by the Slovene Ministry of Higher Education, Science and Technology. US is supported by a fellowship from the David and Lucile Packard Foundation, NASA grants NAG5-1993, NASA NAG5-11489 and NSF grant CAREER-0132953. AT is supported by the National Science Foundation (NSF) under grants No. AST-0206216 and AST-0239759, by NASA through grants NAG5-13274 and NAG5-12326, and by the Kavli Institute for Cosmological Physics at the University of Chicago.

REFERENCES

- Berlind A. A., Weinberg D. H., 2001, in astro-ph/0109001
Blanton M. R. et al., 2003, ApJ, 592, 819
Brainerd T. G., Specian M. A., 2003, ApJ, 593, L7
Collister A. A., Lahav O., 2005, MNRAS, 361, 415
Cooray A., 2004, MNRAS, 348, 250
Cooray A., Sheth R., 2002, Phys. Rep., 372, 1
Diemand J., Moore B., Stadel J., 2004, MNRAS, 352, 535
Ghigna S., Moore B., Governato F., Lake G., Quinn T., Stadel J., 2000, ApJ, 544, 616
Guzik J., Seljak U., 2002, MNRAS, 335, 311
Jenkins A., Frenk C. S., White S. D. M., Colberg J. M., Cole S., Evrard A. E., Couchman H. M. P., Yoshida N., 2001, MNRAS, 321, 372
Jing Y. P., Börner G., 2004, ApJ, 617, 782
Kaiser N., 1987, MNRAS, 227, 1
Kang X., Jing Y. P., Mo H. J., Börner G., 2002, MNRAS, 336, 892
Klypin A., Gottlöber S., Kravtsov A. V., Khokhlov A. M., 1999, ApJ, 516, 530
Kravtsov A. V., Berlind A. A., Wechsler R. H., Klypin A. A., Gottlöber S., Allgood B., Primack J. R., 2004, ApJ, 609, 35
Kravtsov A. V., Klypin A. A., 1999, ApJ, 520, 437
Li C., Jing Y. P., Kauffmann G., Boerner G., White S. D. M., Cheng F. Z., 2005, ArXiv Astrophysics e-prints
Mandelbaum R., Tasitsiomi A., Seljak U., Kravtsov A. V., Wechsler R. H., 2004, ArXiv Astrophysics e-prints
McKay T. A. et al., 2002, ApJ, 571, L85
Nagai D., Kravtsov A. V., 2005, ApJ, 618, 557
Navarro J. F., Frenk C. S., White S. D. M., 1996, ApJ, 462, 563
Percival W. J. et al., 2001, MNRAS, 327, 1297
Prada F. et al., 2003, ApJ, 598, 260
Scoccimarro R., 2004, Phys.Rev.D, 70, 083007
Seljak U., 2001, MNRAS, 325, 1359
Sheth R. K., 1996, MNRAS, 279, 1310
Sheth R. K., Diaferio A., 2001, MNRAS, 322, 901
Sheth R. K., Tormen G., 1999, MNRAS, 308, 119
Tasitsiomi A., Kravtsov A. V., Wechsler R. H., Primack J. R., 2004, ApJ, 614, 533
van den Bosch F. C., Norberg P., Mo H. J., Yang X., 2004, MNRAS, 352, 1302
White M., 2001, MNRAS, 321, 1
Yang X., Mo H. J., van den Bosch F. C., Weinmann S. M., Li C., Jing Y. P., 2005, MNRAS, 362, 711
York D. G. et al., 2000, AJ, 120, 1579
Zehavi I. et al., 2005, ApJ, 630, 1
Zentner A. R., Berlind A. A., Bullock J. S., Kravtsov A. V., Wechsler R. H., 2005, ApJ, 624, 505
Zheng Z. et al., 2004, ArXiv Astrophysics e-prints

This paper has been typeset from a $\text{\TeX}/\text{\LaTeX}$ file prepared by the author.